Journal of Environmental Chemical Engineering 11 (2023) 109687

Contents lists available at ScienceDirect

Journal of Environmental Chemical Engineering

journal homepage: www.elsevier.com/locate/jece

The leaching behaviors of lead, zinc, and sulfate in pyrite ash contaminated soil: mineralogical assessments and environmental implications

Yikai Liu [a], Simone Molinari [a,*], Maria Chiara Dalconi [a], Luca Valentini [a], Giulia Ricci [a], Claudio Carrer [b], Giorgio Ferrari [c], Gilberto Artioli [a]

[a] Department of Geosciences and CIRCe Centre, University of Padua, via G. Gradenigo 6, 35129 Padua, Italy
[b] Magistrato alle Acque di Venezia Ufficio Tecnico Antinquinamento Laboratorio CSMO, Padova, Italy
[c] Mapei S.p.A., via Cafiero 22, 20158 Milan, Italy

ARTICLE INFO

Editor: Chao He

Keywords:
Contaminated soil
Potentially toxic elements
Solid waste
PH-dependent leaching
Geochemical modeling

ABSTRACT

Contaminated soil with high mobility of potentially toxic elements (PTEs) can threaten the environment and human health. Precisely quantifying trends in PTEs accumulation in the soil under changing pH conditions is essential to minimize potential exposure. However, this has long been a hard-to-monitor subject experimentally due to the relatively low content of PTEs and the lack of detailed knowledge of the minerals that control PTEs' leaching. Here we profoundly investigate the critical role of soil mineralogy in PTEs release and predict the leaching behavior of PTEs by exploiting the modeling approach. The investigated sample comes from a brownfield site devoted to fertilizers production. Hematite, jarosite, and gypsum are the major mineralogical phases, with zinc sulfate, anglesite, kintoreite, and Pb-bearing jarosite being identified as the dominant Pb and Zn phases. pH-dependent leaching tests in combination with geochemical modeling were used to reveal the potential leaching mechanisms and contaminants solubility-controlling phases at pH ranging from 1 to 12. The experimental and modeling results both demonstrated that Pb and Zn have an amphoteric leaching behavior, with the lowest leached concentrations at the neutral/alkaline region around pH values from 8.0 to 10.0. The calculated saturation indexes suggest that Pb retention is controlled by anglesite, cerussite, and hydrocerussite, while Zn retention is attributed to zinc carbonates and hydroxides. Further, jarosite and ferrihydrite may play a role in Pb and Zn retention. In comparison, the sulfate release increases with pH values, which is governed by the equilibrium of jarosite, gypsum, and anglesite. The overall results highlight the value of converging experimental-geochemical modeling approaches to gain a deeper understanding of PTEs' release and retention, which is difficult to reveal through experiments alone. These advances may be pivotal in the sustainable management and design of remediation strategies.

1. Introduction

Over the past decades, as a consequence of fast rates of urbanization and industrialization, the discharged potentially toxic elements (PTEs)-containing solid waste have been proven detrimental to soil health [1]. The biological and geochemical cycles may play a critical role in the abundance and redistribution of PTEs in the stockpile sites, with the most commonly encountered trace metal contaminations, including Cd, As, Pb, and Zn, as well as sulfates [2,3]. The former may cause serious neurological diseases and life-threatening cancers [3], whereas the sulfate ions may cause taste impairment and laxative effects [4]. Noteworthy, many solid waste storage sites, such as pyrite ash [5], phosphogypsum [6], and fly ash [7] stockpile regions, are generally more vulnerable because of their location (situated near sensitive aquatic ecosystems) and unstable nature [3]. Although many in- or ex-situ attempts have been adopted to limit and prevent the mobility of these toxic elements, finding applicable management options and overcoming the technical limits is still a challenge due to the presence of impurities which may deteriorate the properties and shorten the service life of the immobilized products [8,9]. For instance, the presence of Pb and Zn is known for its negative influence on the rate of hydration in cementitious systems [10]. Hence, waste stockpiling is still a prevalent method that is still massively used in many countries, but the associated problems, including the degradation of soil and the resultant loss of crop

* Corresponding author.
E-mail address: simone.molinari@unipd.it (S. Molinari).

https://doi.org/10.1016/j.jece.2023.109687
Received 14 December 2022; Received in revised form 15 February 2023; Accepted 12 March 2023
Available online 13 March 2023

yield, have aroused great concern in society [3]. Previous publications suggest that over 340,000 contaminated sites in Europe require immediate treatment, with the most frequent contaminants being trace metals and mineral oils [11,12]. Meanwhile, previous studies have confirmed that the deposited trace metals-bearing particulates would generate varied mineralogical structures containing sulfides, oxides, and silicates, during the stockpiling process, which are driven by the factors such as seasonal wet-dry cycles, geogenic differences, and anthropogenic activities [3,13]. Such processes tend to induce the trace metals to reach a dynamic equilibrium, with the bulk of trace metals may persist in the solid phases of the pedosphere for extended periods due to most of the trace metals remaining non-biodegradable in the soil [14–16]. For example, Contessi et al. [10] found that lead (Pb) in the pyrite ash disposal sites is likely to be hosted in the form of anglesite ($PbSO_4$) because of weathering-induced oxidation. Compared with pyrite, which is a relatively resistant mineral to both acidic and alkaline attacks, the oxidized products would promote the leaching and mobility of Pb. Fazle Bari et al. [17] illustrated that the formation of tooeleite ($Fe_6(AsO_3)_4(SO_4)(OH)_4{\cdot}4\ H_2O$), identified as the dominant arsenic (As) containing minerals in abandoned mine soils, might enhance the solubility of As. Also, in the lead/zinc (Pb/Zn) smelter contaminated soil, Zn incorporation into apatite ($Ca_5(PO_4)_3OH$), wollastonite ($CaSiO_3$), and kaolinite ($Al_2Si_2O_5(OH)_4$) structures and/or precipitated as pyroxene ($XY(Si, Al)_2O_6$, X represents Ca, Na, Fe, Mg, and Zn and Y represents ions of smaller size) and zinc oxide (ZnO) was observed [18]. Therefore, contaminated soil can not only be considered a sink, but also a source of pollution with a great potential for transferring contaminants to the groundwater, the food chain, and the human body [19]. Moreover, the solubility of these PTEs-bearing minerals, as well as their bioavailability and activity in terrestrial ecosystems, is strongly influenced by the soil pH of the storage sites [3,10]. Although a wide range of literature indicates that even small changes in pH may significantly affect the mobility of PTEs with cascading effects on communities and environments [3,10,20], there are important gaps in our understanding of changing pH conditions as a driver of the dynamics of PTEs-bearing minerals in the ecosystems. Before deploying remediation technologies, it is crucial to study the origin and fate of PTEs in dynamic environmental conditions, particularly easily mobile forms, plus leaching behavior and total concentrations of these PTEs [21].

To achieve this goal, detailed characterizations are necessary prerequisites to provide a fundamental understanding of the fate of hazardous contaminants. Concurrently, many laboratory works have been carried out to fill the knowledge gap in the mineralogy and chemistry of phases incorporating contaminants [18,22,23]. With the scope of simplifying the analysis process, some works attempted to use the experimental datasets required in prior literature to reconstruct the transformation by simplified artificial systems [24–26]. But the extrapolation from the laboratory findings to the real cases is usually far from satisfactory. Another major limitation is the detection limit of the routinely employed analytical techniques [27] (e.g., the XRD technique is not sensitive to trace elements in solid-solution phases or to ionic species adsorbed on mineral surfaces). Therefore, individual analytical methods are not always suitable or sufficient for overall knowledge of the fate and long-term behavior of mineral phases controlling toxic elements released in such a complex pollutants-soil system, especially since this dual system will suffer complex environmental impacts [28,29]. Geochemical simulations could be the key to overcome the complexity of linking the potential release of hazardous chemical constituents with soil mineralogical and deeply understanding long-term environmental impacts that affect surrounding groundwater. Currently, several attempts have been conducted to explore how mineralogical factors control the leaching behaviors of toxic elements. Bisone et al. (2017) used a geochemical assessment to characterize the spatial variability of toxic elements in stocked phosphogypsum at varying time periods and pH values [6]. Other researchers also tried to reconstruct the leaching profiles of metals (e.g., Pb, Zn, Cu, and As) as a function of pH values [30,31]. The above geochemical assessments of leaching showed good consistency with experiments, but it is not a common practice to perform the geochemical modeling construction based on the bulk experimental characterization (e.g., XRD), even though this mineralogical information is of paramount importance in determining which minerals dissolved during the leaching procedures. Therefore, in this study, we tend to explore the role of dissolving/precipitating mineralogical phases through the bulk XRD characterization, which is a missing key element in understanding the factors controlling the dispersion of contaminants and overcoming the limitations of the demanding experimental procedures [32,33].

The main objective of the present study is to bridge the knowledge gap of pH-dependent leaching characteristics and associated mineralogical information of Pb and Zn-contaminated soils. The chemical and mineralogical compositions of the contaminated soil were first characterized through a multi-technique approach based on XRD, XRF, SEM/EDS, and Raman analyses. Afterward, the pH-dependent leaching of hazardous (Pb, Zn, and sulfate) and major elements (Fe) was explicitly studied in the pH range of 1.02–12.02. In order to elucidate the impacts of mineralogical compositions on the partitioning of chemical species between the solid and aqueous phases at different pH values, geochemical modeling was performed to predict the leaching behavior. Meanwhile, the leaching residues were analyzed to give corroborating insight into the predominant solubility-controlling mechanisms. The combination of traditional characterization approaches with geochemical modeling may be helpful to better understand the influence of different parameters on environmental risks and provide a reliable, low-cost, and much less time-consuming instrument to evaluate suitable remediation and management techniques for contaminated soil.

2. Materials and methods

2.1. Sampling process

The soil used in this work was excavated from an abandoned fertilizer production facility in Italy, which is now used as a storage site for the solid waste generated by pyrite roasting, sulfuric acid production, and phosphorus-based fertilizer production. The contaminated soil was collected following a systematic sampling grid from the surface to 2.5 m depth covering the whole area of around 0.11 km^2. In this work, the soil was mainly composed of black pyrite ashes. The soil sample was placed in a polyethylene bag and then transported to the laboratory. Then the sample was air-dried, ground, and passed through a 2 mm mesh sieve prior to the following characterization experiments. The soil moisture content was calculated by drying the soil in an oven a 105 ± 5 °C according to UNI 12457–4:2004 [34] and resulted below 1%.

2.2. Characterization methods

Prior to characterization, the sieved soil was divided by using coning and quartering to obtain a representative sample. The solid sample was digested following the procedure reported by [35]. HF, HNO_3, HCl, and H_3BO_3 (AppliChem GmbH, Darmstadt, Germany) were used at high purity levels for trace metal analyses. Before the XRD analysis, the divided fraction was ground in an agate mortar and then micronized for 10 mins (McCrone micronizing mill, RETSCH Inc., Haan, Germany) in order to reduce the effect of the preferred crystallographic orientation [36]. The mineralogical composition of the micronized sample was determined by XRD Rietveld analysis [37]. Diffraction measurements were performed using a Malvern Panalytical X'Pert Pro diffractometer operating in Bragg-Brentano geometry. The instrument setup is provided in Table.S1. Diffraction data were acquired from 3° to 84° 2θ, with a step interval of 0.017° and an equivalent counting time of 100 s per step. Known amounts of ZnO (ACS Reagent, Thermo Fisher Scientific Inc., Waltham, USA) were homogeneously mixed with the samples as an internal standard. Qualitative and quantitative analyses of the collected

XRD patterns were executed using Highscore Plus and Profex [38], respectively. The elemental composition of contaminated soil was determined with XRF (PW1480, Philips, USA). SEM/EDS investigation (CamScan MX3000, Applied Beams, USA) was performed on the polished and carbon-coated sections of contaminated soil. Detailed Raman investigation (DXR Raman microscope, Thermo Electron, USA) was conducted with a laser operating at 532 nm.

2.3. pH-dependent leaching tests and ion concentrations determination

The pH-dependent leaching tests were performed on the sieved soil following the EN 14429:2015 (British Standards Institution, 2015) standard, consisting of a series of parallel batch extractions tests with increasing pH values. The analytical reagent nitric acid (HNO_3) or sodium hydroxide (NaOH) was used to adjust the pH values of the leachate. The amount of used HNO_3 and NaOH are given in Fig.S3. Eluates were filtered at 0.45 μm and analyzed for Fe, Pb, and Zn by inductively coupled plasma mass spectrometry (ICP-MS, ELAN DRC II, Perkin, Elmer) following method UNI EN ISO 17294–2 (2016). The detection limit was 5.0, 0.1, and 1.0 μg L^{-1}, respectively. Sulfate concentration was measured by Inductively Coupled Plasma Optical Emission spectroscopy (ICP-OES, OPTIMA 2100 DV Perkin Elmer) following method CNR IRSA 5(2) (1985). The detection limit was 1 mg L^{-1}. The ICP-MS analysis of all the other quantified elements is reported in Table S4. The certified standard NIST-SRM 2711a (Montana II Soil) from NIST (National Institute of Standards and Technology, Gaithersburg, MD, USA) was used to validate the analytical methodology. All analyses were performed in triplicate.

2.4. Geochemical modeling

Geochemical simulations were conducted using the software PHREEQC [39] with two thermodynamic databases from MINTEQ [40] and Lawrence Livermore National Laboratory (LLNL). The initial mineralogical input was based on XRD quantification and SEM/EDS characterization. Besides, additional mineral assemblages were given according to previous literature. The description of the initial input data is shown in Table.S2. The calculations (pH values range from 1 to 13) were based on the pH-dependent leaching tests, using NaOH and HNO_3 as the pH control agents. Meanwhile, the soil XRD result obtained was used as a starting point to select the set of mineral phases to take into account in the modeling approach. The XRD characterizations of the residues were used to constrain the maximum amount of minerals that can dissolve [41,42]. Based on the quantification results of the residues at the overall pH range, the maximum amount of jarosite that would participate in the dissolution process was predictably assumed as 40 wt %.

3. Results

3.1. Characterization of the contaminated soil

The XRD mineralogical investigation (Fig. 1) illustrates that hematite (Fe_2O_3) is the main crystalline phase present in the sample, with a concentration of 72.0 wt%. The high content of hematite is consistent with the findings of previous works on soils sampled in pyrite ash disposal sites [5,10]. The Pb-containing minerals are identified as anglesite (0.6 wt%) and kintoreite ($PbFe_3(PO_4)(SO_4)(OH)_6$, 1.7 wt%). The other observed minerals are mainly sulfates and silicates: gypsum ($CaSO_4{\cdot}2\ H_2O$, 15.3 wt%), jarosite ($KFe_3(SO_4)_2(OH)_6$, 7.6 wt%), and quartz (SiO_2, 2.8 wt%). The chemical composition from the XRF (Table. S3) shows Fe_2O_3 (83.1 wt%), CaO (8.6 wt%), and SiO_2 (6.4 wt%) as major elements, which validates the XRD characterization as the hematite, gypsum, and quartz being the principal components. The detected P_2O_5 (0.5 wt%) and K_2O (0.2 wt%) agree with the presence of kintoreite and jarosite. Minor contents of Al_2O_3 and Na_2O can be related to the clay minerals from the soil. The trace metal content of the contaminated soil is presented in Table.S4, showing a very high concentration of Pb (11910 ± 714 mg/kg) and a minor content of Zn (582 ± 43 mg/kg).

The SEM images (Fig. 2a, b, and c) further evidence the presence of hematite, jarosite, gypsum, quartz, and anglesite. Besides forming sparingly soluble anglesite at acidic conditions, Pb was found in complex exsolution/intergrowths textures in amorphous Fe oxide phases (Fig. 2d and e) and incorporated in the Fe-K-S-Pb oxide rims in a compact form along the edges of the structures (Fig. 2 f and g). A previous study also characterized the incorporation of Pb to Fe oxide phases [10], and an adsorption mechanism was accordingly given to explain this observation. Therefore, the presence of Fe-K-S-Pb oxide rims could imply Pb incorporation within the jarosite crystal structure [43,44]. In addition, the fate of Zn was related to the formation of sulfur minerals, as a Zn-Fe-S assemblage was observed in Fig. 2i. But as a minor component, it is hard to assess the exact origins of this assemblage, which could represent a residue of the primary ore or a precipitated secondary phase.

To analyze the Pb distribution mechanisms in the contaminated soil, Raman spectroscopy was used to examine the area with high Pb concentration presented in Fig. 2d and g. In addition to hematite (Fig. 3a and b) confirmed by previous XRD, the Raman spectra show the presence of clear vibration bands that can be associated with different Pb-containing phases (Table.S5). In Fig. 3c, the sulfate anion is characterized by the bands at 1160, 1100, 1004, 620, and 437 cm^{-1} [45]. The bands at 976, 557, and 335 cm^{-1} are assigned to the vibration of PO_4^{3-} [46]. Although previous studies have reported that four sharp bands can be observed at the wavenumber range from 420 to 480 cm^{-1} due to the $\nu_2\ PO_4^{3-}$ bending modes, these bending modes could suffer the influence

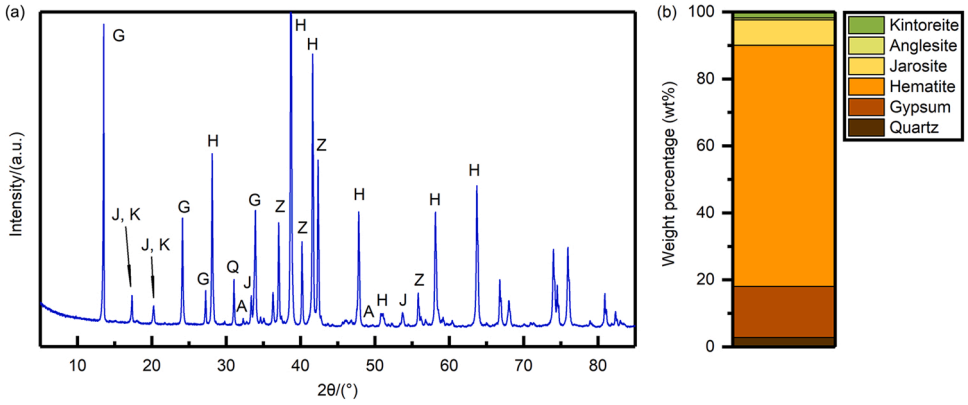

Fig. 1. XRD characterization of studied soil sample. (a) XRD pattern of the studied sample with the abbreviations A: anglesite, G: gypsum, H: hematite, J: jarosite, K: kintoreite, Q: quartz, and Z: zincite (internal standard) and (b) quantification results after subtracting the internal standard.

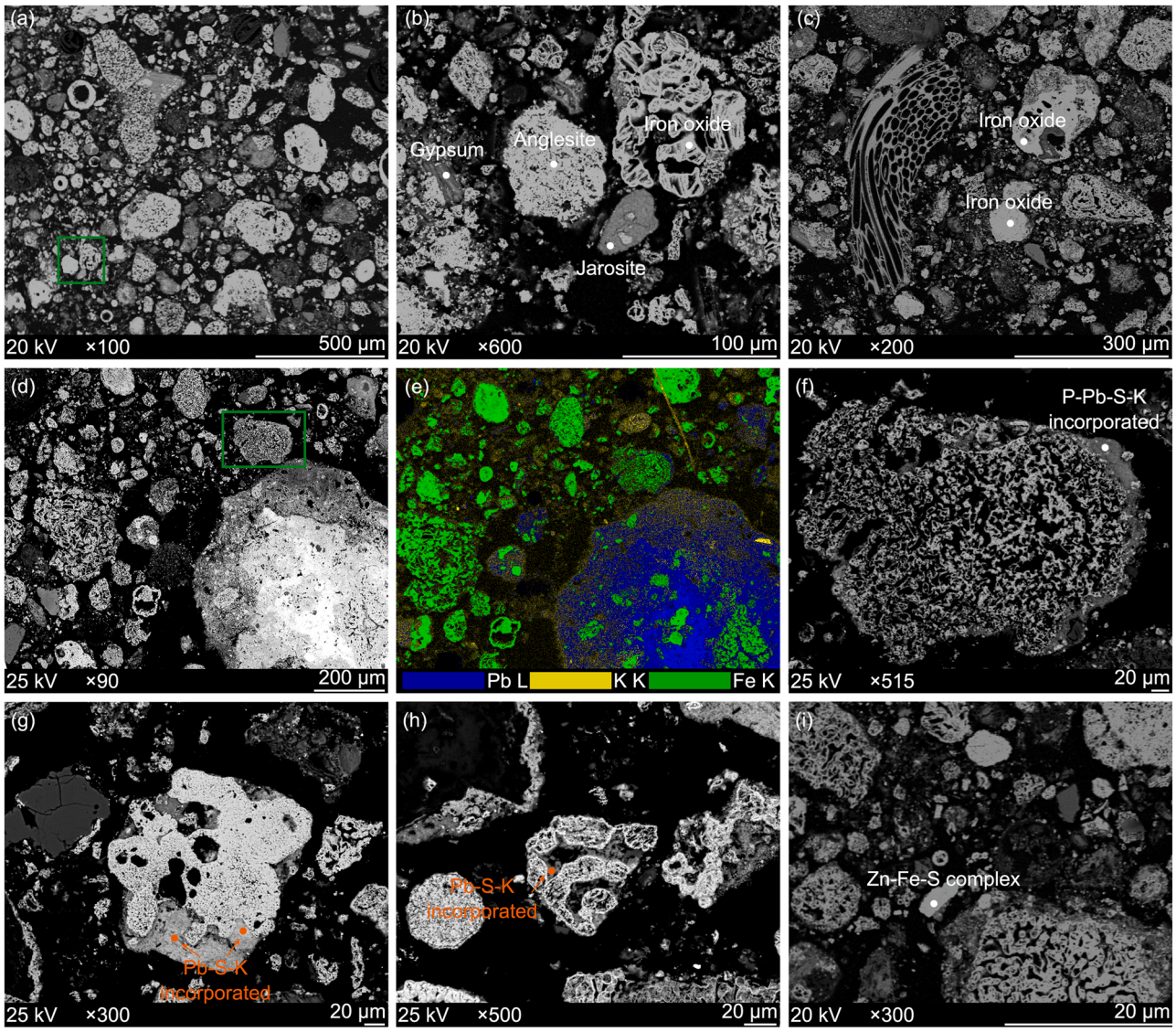

Fig. 2. SEM micrographs of the sample. (a) backscattered scanning electron (BSE) microscopy image of contaminated soil; (b) BSE image showing the presence of anglesite;(c) BSE image implies the iron oxide; (d) BSE image demonstrates the distribution of Pb; (d) elemental mapping of lead, potassium, and iron attributing to image d; (f) the magnified BSE image corrected to the green rectangle marked area in image d, indicating a Pb-incorporated structure; (g) and (h) the compacted Pb-bearing assemblages; and (i) BSE image shows the Zn-Fe-sulfate assemblage.

of overlap [45]. Hence the Pb concentrated area in Fig. 2d and Fig. 3a implies the presence of kintoreite. In comparison, the band positions given in Fig. 3b and d showed almost no changes to the standard K-jarosite [47]. It is probable that the low concentration of Pb ions incorporated into the structure and the multiple overlapping bands due to the complexity of jarosite prevent any significant band shift related to Pb incorporation into jarosite [45,48]. In addition, another study has shown that incorporating Pb will significantly broaden the bandwidths of peaks at 1000 and 1005 cm^{-1} and raise three split bending modes at the low-wavenumber region (approximately at 436, 452, and 476 cm^{-1}) [49]. However, these abovementioned vibration modes promiscuously overlapped with the SO_4^{2-} and O-Fe vibration profiles. Comparing the EDS point analysis (Fig.S1) with the Raman investigation, we inferred that the presence of Pb-bearing jarosite was entirely obscured by prevailing Raman bands of K-jarosite and hematite. Meanwhile, based on the optical microscopy and SEM images, it is likely that Pb species are combined with K-jarosite and hematite without distinct boundaries. Although the literature suggests that the alunite-jarosite family could hypothetically function as collectors of Pb in the form of plumbojarosite ($Pb_{0.5}Fe_3(SO_4)_2(OH)$) [50], the Pb presence in our samples is more likely to be assigned by the co-existing mechanisms (adsorption on the surface and/or coprecipitation in the jarosite structure), because the characteristic peaks of plumbojarosite were not found in the XRD pattern (Fig. 1a). Therefore, the occurrence of Pb (Fig. 2d and e) may be related to the phase transformation (for instance, anglesite and K-jarosite) through the dissolution/precipitation process or solid-state recrystallization during the weathering process [43].

3.2. pH-dependent leaching tests

Fig. 4 illustrates the concentration of released Pb, Zn, Fe, and SO_4^{2-} with the acid/base addition to the solution in contact with the contaminated soils. When using deionized water as the leachate (at pH 4.6), the leachability of the tested elements showed that the contaminated soil should be classified as hazardous waste, with all the concentrations being significantly higher than the limits established by Italian laws (Table.S6). The leaching of the studied trace metals (Pb, Zn, and Fe) showed a strong dependence on the pH values, indicating that the contaminated soil is susceptible to changing conditions of the stockpile. At the pH value of 1.98, the highest concentrations of Pb, Zn,

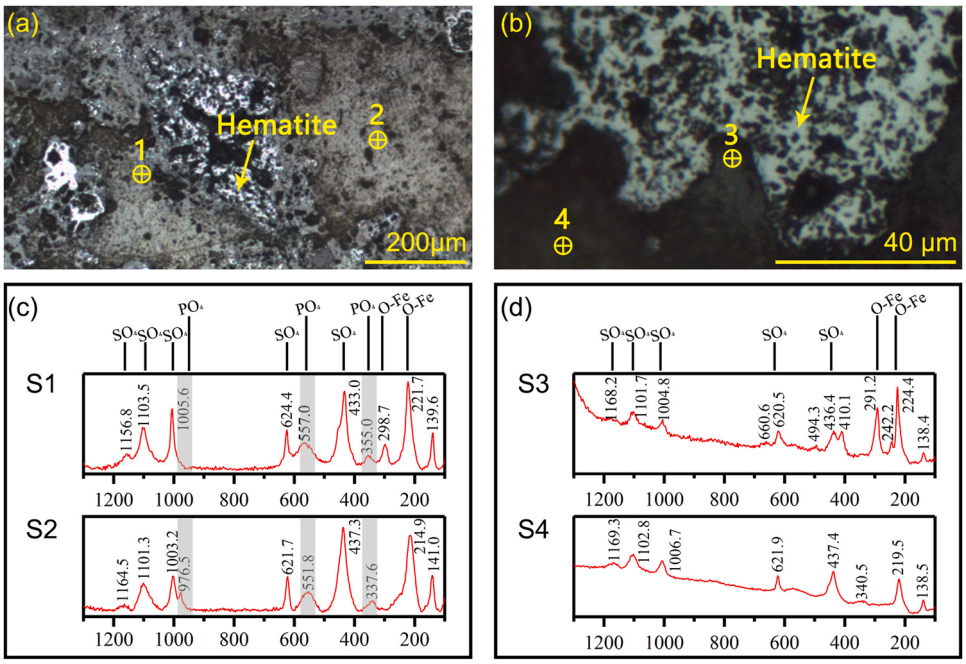

Fig. 3. Raman spectra of the contaminated soil. (a) and (b) Optical microscope images of the tested area correlated to Fig. 2d and g, respectively; (c) and (d) Raman spectra of the marked point, with the abbreviation S1 representing spot 1.

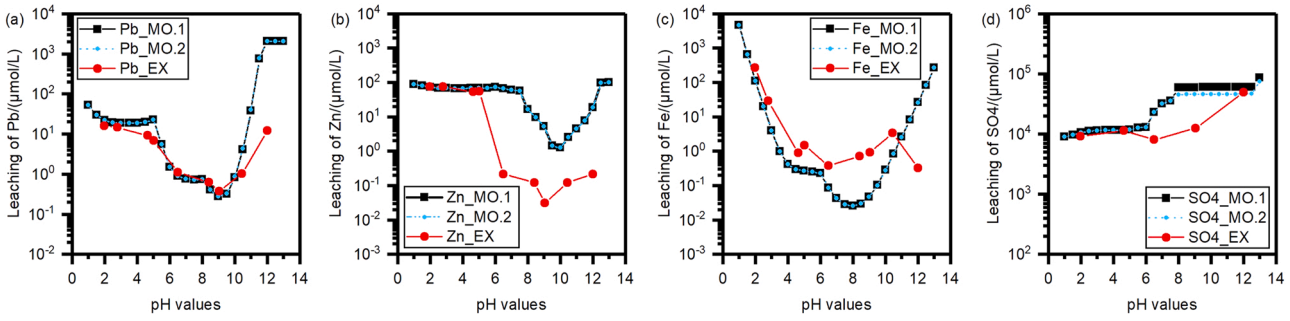

Fig. 4. pH-dependent leaching results of Pb (a), Zn (b), Fe (c), and SO_4^{2-} (d) from experiments and simulations. The abbreviation EX means the experiments. MO.1 and MO.2 represent the geochemical modeling without or with jarosite dissolution limit.

and Fe in the leachate were reached at 1.59×10^1, 7.49×10^1, and 2.69×10^2 μmol/L. The minimum release of Pb (0.38 μmol/L) and Zn (0.30×10^{-1} μmol/L) was found at the pH value of 9.04. However, with the increase in pH values, Pb and Zn showed an upward tendency in the release under alkaline conditions. These amphoteric Pb and Zn leaching profiles were also observed in the research of Contessi et al. [10], Cappuyns et al. [31], and Jarošíková et al. [51]. The enhanced element release at basic conditions was due to the occurrence of specific dissolution of minerals (e.g., the transformation of Pb/Zn bearing carbonates to hydroxides) [52] and desorption reactions of elements from reactive surfaces (e.g., Pb/Zn may desorb from Fe-oxides surfaces and favor the formation of hydroxyl-complexes). [31]. By contrast, the release of Fe at the neutral/alkaline conditions fluctuated approximately from 0.32 to 3.40 μmol/L, which was probably related to the formation of iron hydroxide [31]. Besides, the increasing leachability of SO_4^{2-} was only observed under alkaline conditions, with the concentrations being constant at around 10^4 μmol/L in the acidic and neutral regions.

3.3. Mineral composition after leaching

To reveal the dissolution/precipitation of the mineralogical phases at different pH values, the solid residues after the leaching tests were collected for the mineralogical characterization. From quantitative phase analysis of the XRD patterns (Figs.S2 and 5), it can be seen that quartz and kintoreite are not affected by pH variation, with the concentration remaining approximately constant in the studied pH ranges. Despite a decrease in hematite appearing in the near-neutral region (Fig.5c and d), the mass fraction of hematite still dominates the total amount of phases. It is to note that the weight fraction variation obtained by Rietveld's quantitative analysis of the soil samples before and after leaching procedures can be directly compared only, assuming that the solid mass of the sample stays constant. But during the leaching tests, part of the samples is dissolved, such that the constant mass assumption is invalid. Therefore, the weight fraction of the quantified minerals may interplay with the dissolution and precipitation of other phases (for instance, the hematite fraction quantified by the XRD patterns may be influenced by the dissolution of gypsum, thereby its weight percentage increased massively at acidic conditions, see Fig.5a and b). Further, anglesite exhibits a higher solubility in the alkaline pH ranges. This observation is consistent with findings of previous works where anglesite is considered the most stable Pb-bearing phase when pH < 5.5 [10, 53]. Regarding gypsum, the XRD results illustrate that it is abundant at neutral pH values, with 4.2, 14.6, and 11.0 wt% being present at pH values of 1.26, 6.5, and 12.02, respectively. Jarosite was preserved at

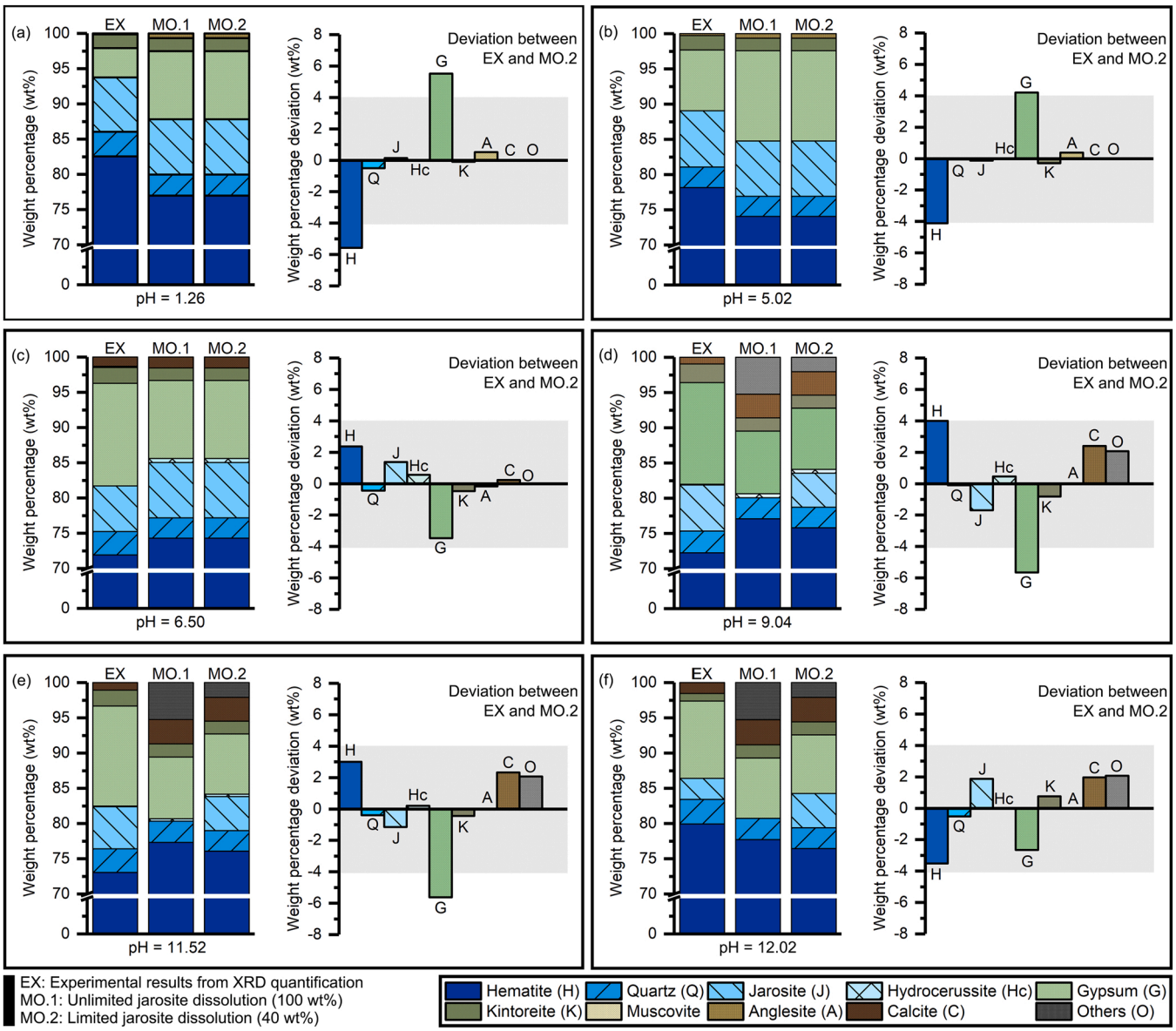

Fig. 5. Quantified mineral assemblages of the residues from the XRD patterns and Phreeqc models and the correlated deviation. The leachate pH values at (a) 1.26, (b) 5.02, (c) 6.50, (d) 9.04, (e) 11.52, and (f) 12.02. The "Other" in the simulation is the weight percentage accumulation of $Fe(OH)_3$ and $Zn(OH)_2$ matrix. The marked gray rectangle represents the XRD limitation (± 2 wt%). The predicted weight percentage of hydrocerussite is the accumulation of cerussite and hydrocerussite.

highly alkaline conditions, even though it was confirmed that it has a higher solubility when pH values > 4.5 [54]. In the residues collected from the leachate at the pH of 12.02, 3.0 wt% of jarosite was quantified in the XRD pattern (Fig.5f), indicating that approximately 40% of jarosite dissolved. Previous work suggested that jarosite preservation at high pH values could be explained by the formation of nanoparticles of secondary iron oxide phases on the jarosite grain surfaces, which inhibits subsequent jarosite dissolution and does not resorb either K or SO_4 ions [55]. Similar observations are also presented in the original soils (as shown in Fig.2 g and h). Approximately 1.0 wt% of calcite was characterized in the XRD pattern at pH values higher than 6.5. The occasionally found muscovite (pH 9.04, 0.6 wt%) could be related to the original soil from the stockpile site.

3.4. Geochemical modeling: the leaching profiles and phases equilibrium

To determine which processes and minerals control the release of hazardous contaminants, experimental results (the mineralogical composition of the residues and pH-dependent leaching tests) were combined with geochemical modeling. Based on the preliminary characterization, some basic modeling assumptions were adopted: (1) quartz is assumed insoluble during the studied pH range, as derived by quantitative analysis of XRD data indicating that this phase stays constant (Fig.5a and f); (2) since hematite formation is favored at high temperatures and low salinity [56], the precipitation of this phase was not envisaged in the model; (3) in the first simulation (MO.1), jarosite was assumed to participate entirely in the dissolution/precipitation reactions and in the second approach (MO.2), a dissolution limitation coefficient, controlling the maximum amount of jarosite allowed to dissolve in the model, was set to simulate the effect of coating film (physical protection of iron oxide) mentioned in the previous sections. Based on the experiments (Fig.5a), the parameter was set as only 40 wt % of jarosite would participate in the dissolution/precipitation reactions; (4) due to lack of knowledge of the thermodynamic data of kintoreite, in this work, this mineral was assumed stable. Additionally, the saturation index (SI) was used to determine whether the solution is

saturated (equilibrium, SI = 0) or undersaturated (mineral dissolution, SI < 0) with respect to the given Pb- and Zn-bearing minerals.

The predicted Pb, Zn, and Fe leaching profiles (Fig.4a, b, and c) illustrate that both simulations can describe the pH-dependent leaching behavior of the tested systems. Noteworthy, compared to the acidic conditions, the leaching of Pb and Zn in harsh alkaline conditions should be carefully investigated since a previous work demonstrated that the leaching of Pb under alkaline conditions (pH>11) could be several magnitudes higher than the acidic conditions [10]. From the predicted mineralogical composition (Fig.5) and SI values (Fig.6a), from near-neutral to moderately alkaline conditions, the Pb retention is closely related to the equilibrium of anglesite, cerussite ($PbCO_3$), and hydrocerussite ($Pb_3(CO_3)_2(OH)_2$). In contrast, the plumbojarosite is undersaturated in the whole pH range. These observations ascertain the findings in previous research [52]. The detected Pb release at this pH range can be explained by the formation of Pb-containing stable aqueous complexes (with CO_3^{2-}, SO_4^{2-}, and OH^-). In contrast, at pH values over 12.5, all the Pb-bearing phases are undersaturated, indicating that Pb is prone to be preserved in the solution in the form of lead hydroxide complex [57], which is consistent with the amphoteric leaching behavior. In Fig.6b, it can be seen that the retarded release of Zn at near-neutral conditions is due to the precipitation of carbonates (smithsonite and $ZnCO_3{\cdot}H_2O$) and hydroxides ($Zn(OH)_2$). But at acidic conditions, the aqueous Zn speciation is dominated by Zn^{2+} and $ZnSO_4$ instead of the zincosite precipitation. Similar to what was observed for Pb, Zn in the alkaline leachates occurred in the form of aqueous hydroxides species ($Zn(OH)_4^{2-}$ and $Zn(OH)_3^-$).

In addition, the assumed limitation of jarosite dissolution (MO.2) reduced the deviation of SO_4^{2-} leaching data between the experimental and modeling results (Fig.4d), indicating that except for the gypsum and anglesite dissolution, the jarosite is also a predominant source of sulfate contaminants. Although the deviation of the SO_4^{2-} leaching was slightly improved by the assumption of limited jarosite dissolution, a significant difference still can be observed at the pH range from 7 to 12, which is not in agreement with the experimental findings. Hence, although the thermodynamic database used in this work is widely recommended, it is clear that the given log K value has overestimated the solubility of gypsum and tended to estimate sulfate concentrations that were two to three orders of magnitude higher than the experiments. By comparing the predicted mineralogical compositions of the residues with the experimental results (Fig.5), the geochemical approach demonstrates a great potential to quantitatively describe the transformation of the minerals, with a good agreement between the phases characterized by XRD and the predicted minerals by geochemical modeling. A major discrepancy is detected in the gypsum estimation, as approximately 5.5 wt% of maximum deviation in the residues at particularly acidic conditions (pH 1.26, Fig.5a). This discrepancy is slightly reduced at neutral and alkaline conditions, as shown in Fig.5c, with a difference between experimental and modeling results of 3.4 wt%. It is to note that geochemical modeling is capable of detecting such small variations of the PTEs-containing phases (< 1 wt%), which is hard to be revealed by the XRD mineralogical analysis. As shown in Fig.4a, when the pH increases to neutral conditions (pH values 6–9), which is unsuitable for the anglesite stability [10] and the XRD characterization revealed the dissolution of anglesite (Fig.S2). The experimental XRD data did not identify mineralogical phases responsible for the retention of Pb at this pH range, with none of the lead-bearing crystalline phases being detected. The geochemical modeling results, along with previous investigations [58–60], suggest that the Pb-carbonate phases (hydrocerussite and cerussite) precipitate at neutral conditions (0.57 wt% at pH 6.5, Fig.5c) and then slightly dissolve (0.33 wt% at pH 11.52, Fig.5e) with the increase of pH. Similarly, about 0.010 wt% of Zn hydroxide was expected to precipitate in the residues at a pH of 9.04 (Fig.5d), then the weight percentage slightly decreased to 0.008 wt% (Fig.5e).

4. Discussion

4.1. Reconstruction of the mineral transformations from the fertilizer production and weathering process

With the previous mineralogical and chemical investigations, the distinct phases in the bulk soil provide valuable information to reconstruct the linkage between the stocked wastes and soil. In a typical P-fertilizer manufacturing chain (Fig.7a), the pyrite and apatite ores were

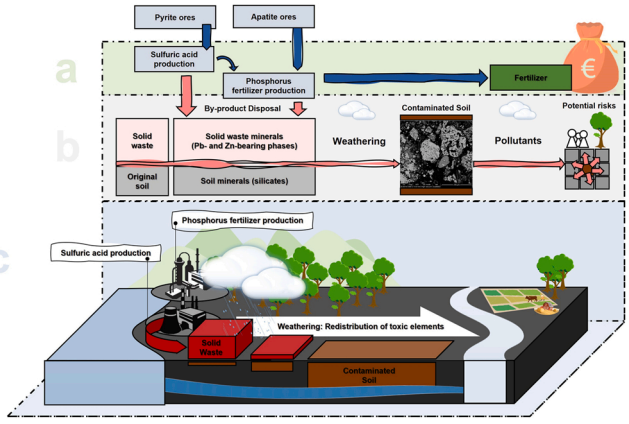

Fig. 7. Schematic cartoon depicting solid waste generation due to industrial activities (a), the transformation of mineralogical phases from stockpiled solid waste and original soil during the long-term weathering process (b), and the overall geographical description of the studied sites (c).

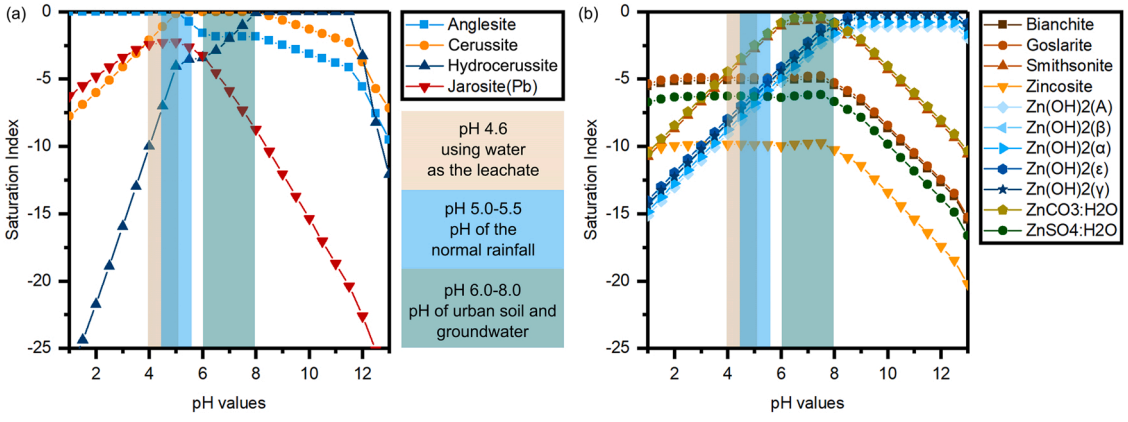

Fig. 6. The SI of Pb-(a) and Zn-(b) bearing minerals from MO.2.

used as the raw materials for sulfuric acid production and the following phosphorus fertilizer production [61,62]. The primary components in pyrite ash are hematite and calcium sulfates, which are naturally occurring minerals in the environment with low toxicity [5,63]. The concentrated pyrite ores are heated to 900 °C to extract the sulfur (mainly in the form of SO_2), leaving a residue consisting mainly of iron oxide [5]. However, the generated by-products, iron oxide (hematite) and sulfates minerals (jarosite), would cover the unreacted pyrite and then preserve a partially reacted pyrite grain [5,64]. Compared to the other co-existing sulfides, the remained pyrite is readily weathered and promotes the oxidation and dissolution of galena (PbS), which is a significant Pb host in the pyrite ores [10]. Therefore, anglesite was present in the contaminated soil systems (Figs.1 and 2b) as a secondary oxidized product from the unreacted grains.

Lead was concentrated along the edges of iron oxides, as observed in Fig.2d, e, and f. The vibrations in the Raman spectra (Fig.3b and d) also show more complexity for these Pb-bearing phases. Previous works have ascertained the observation [65,66] that Pb is partially released from sulfide minerals as vapor during roasting. The volatilized Pb condensed on the external and interior surfaces of the porous iron oxide grains, which have high thermal stability, and formed sulfate precipitates (mainly $PbSO_4$). Then the free ferric ions formed by gradual dissolution are in contact with $PbSO_4$, which are then hydrolyzed to generate Pb-rich jarosite [67]. Further, the SI modeling illustrates that although the SI values of plumbojarosite are increasing and closely approach saturation equilibrium state in the water leaching condition (pH 4.64, Fig.6a), this phase is still undersaturated, and the formation of anglesite is favored. Experimental evidence confirmed that the formation of pure plumbojarosite hardly occurs in ambient conditions (air temperature and neutral pH conditions) [43]. For instance, Forray et al. (2010) synthesized plumbojarosite by the reactions between the $Fe_2(SO_4)_3{\cdot}5\ H_2O$, $Pb(NO_3)_2$, and H_2SO_4 solutions at a temperature of 95 °C. In this case, the observed Pb (Fig.2 f, g, and h) are not associated with the presence of plumbojarosite. The lead distribution in the soil can likely be explained by considering a combination of mechanisms such as incorporation and physicochemical mixtures [43,68]. It has been established that Na- and K-jarosite can act as efficient carriers of Pb because they can incorporate Pb in their crystal structure [69]. Usually, jarosite forms as a product of pyrite oxidation under very acidic conditions. Accordingly, these coprecipitation processes may represent a likely mechanism for incorporating the metal cations present at the interfaces, which would have high mobility at this pH condition (as demonstrated in Fig.4a, approximately at pH>10) in the jarosite structure [50]. Besides, apart from the formation of Pb/Na/K-jarosite compounds, Pb may preferentially precipitate as anglesite (Fig.6a) [43]. The formed anglesite can serve as crystal nuclei for the subsequently precipitated jarosite. In this case, although Pb does not enter the jarosite structure, the anglesite is surrounded by jarosite forming small-scale mixtures. However, because of the complex speciation of Pb, it is hard to assert an exact interaction between the Pb and jarosite.

Regarding the characterized kintoreite, it is hard to ascertain if kintoreite is a gangue mineral originating from the ores or if it is a secondary mineral generated during fertilizer production. Many studies strongly emphasize that the occurrence and aggregation of kintoreite in the impacted soils is most likely a result of the acidity of the stockpile sites and the raw wastes (pH values from 3 to 4). The continuously leached Fe^{3+} and PO_4^{3-} combined with Pb (released mainly from galena) to form kintoreite [70–72]. But some field works also demonstrate that rare kintoreite is present in cavities of quartz gangue [73,74]. Nevertheless, the quantified kintoreite weight fraction almost remained unchanged over the measured pH range (Fig.5), indicating it barely contributes to the Pb leaching profiles. This is also ascertained by the geochemical modeling (Fig.4a), as the assumption was given that the kintoreite will not participate in the precipitation/dissolution reactions, the simulated Pb leaching is still matched with the experiment results. Zinc that occurs in the contaminated soil could mainly be in the minor phases of zinc sulfate (Fig.2i). The distribution of zinc sulfate is associated with the sphalerite present in pyrite ores, which can be oxidized by either dissolved molecular oxygen or ferric iron and then form secondary sulfates or other acid-exchangeable species [22,75]. Meanwhile, with the time and climate conditions, the secondary zinc phases probably continue reacting at high humidity with the atmospheric CO_2 (the stockpile site in this study is a coastal city, as shown in Fig.7c) [59,76]. The detected gypsum is a typical by-product generated from phosphorus fertilizer production [61]. Unlike phases containing metals, gypsum residues are not dangerous for the environment, though the abundance of sulfate would accelerate the migration of metals [77]. Further, with the increase of the pH values, the carbonates and hydroxide phases dominate the Pb and Zn retention.

4.2. Influence of pH values on the geochemical stability of PTEs

As recognized by previous investigations [10,78], pH is one of the most important factors controlling changes in the mineralogical concentration and leachability of PTEs. Hence, the pH-dependent leaching tests can efficiently reveal the fundamental mechanisms, such as possible ion exchange/sorption, complexation, and precipitation/dissolution [79,80]. The results of leaching tests (Fig.4) and the mineralogical study (Fig.5) illustrated that the addition of acid agents caused increased concentrations of Pb, Zn, and Fe in solutions. Noteworthy, over the acidic pH range, Pb was preferentially precipitated as anglesite (Fig.6), but the leaching of Pb was still increased with the pH decrease. By checking the original (unnormalized) mineralogical compositions of the residues in the simulations, only 0.005 wt% weight loss of anglesite was found at the pH value of 1.26 (from 0.621 wt% at pH 5.02–0.616 wt% at pH 1.26), showing that the relatively small changes in weight percentage may cause an increase in the leachate concentration. Therefore, with continuously increased HNO_3 agent fraction in the system, anglesite is expected to dissolve partially and form ion pairs ($PbNO_{3(aq)}^{+}$) [81,82]. Further, Zn is mainly preserved in the acid solutions in the monatomic ion form, accompanied by the minor $ZnSO_{4(aq)}$ complex. At the pH range from 2 to 5, the slight deviation in leaching curves could be attributed to the Pb/Zn-substituted jarosite. There have been previous studies stating the strong affinity of Zn and Pb to Fe-minerals, suggesting that jarosite can efficiently immobilize metals by incorporating the metal ions in its crystal structure [48,67]. Thus, the incorporated Pb and Zn should remain stable in the residues, with a relatively slow-releasing rate (Fig.6a). When the pH values increase to near-neutral conditions, Pb and Zn are preferentially precipitated as carbonates and hydroxides (Figs. 5 and 6). But the simulated leaching profiles can only partly reflect the overall trends (Fig.4b), with minimum Pb and Zn leaching around a pH value of 10. Especially, the measured Zn concentration was one order of magnitude lower than what the model predicted (10^{-1} and 1 μmol/L, Fig.4b). This deviation could be partially explained by the high sorption ability and metal affinity of ferrihydrite [83–85], which is a phase rarely exists as pure precipitation but a highly affinitive host for various foreign elements, such as Si, Al, and Mn [86]. The additional modeling (Fig.S4) also verifies this hypothesis. With the assumption of Zn adsorption onto ferrihydrite, the estimated Zn leachability at pH values from 6 to 10 is slightly optimized compared to MO.1 and MO.2. Therefore, the adsorption competition among Pb, Zn, and other elements may play a crucial role in their mobility in the environment. However, this does not match experimental results since the amorphous content (ferrihydrite) is not observed in the quantification results. Besides, the preservation of Zn could also be related to the porous microstructure of hematite (Fig.2c and f). The Zn may be strongly bound to the crystalline structures of hematite and then preserved without a mineral phase change, which is associated with coupled O–Fe and protonated Fe vacancies [22,87]. In alkaline conditions (pH >10), despite the fact that ferrihydrite sorption mechanisms should theoretically display a role in the Pb and Zn retention, the increase of leaching profiles was observed in this work, also

ascertained by previous investigations [10,52]. The geochemical modeling shows that the increased leaching rate under alkaline conditions can be related to the formation of anionic hydroxo complexes such as $Zn(OH)_3^-$, $Zn(OH)_4^{2-}$, $Pb(OH)_3^-$, and $Pb(OH)_4^{2-}$, suggesting that the adsorped trace metal cations partially dissolved due to the anionic properties of the newly formed hydrolyzed species preclude their sorption onto the negative surface of the ferrihydrite. Similar results are reported by [88] and [20]. Although an increasing trend of Pb and Zn concentrations was observed at this pH range (8−13), their relative leached amounts are still lower than those detected at acidic conditions (pH 1–3, Fig.4a and b), which implies that other factors, such as structural incorporation (isomorphous substitution and occupation of vacant sites of hematite and ferrihydrite), Pb-Fe solid solutions, and mechanical occlusion (Pb-bearing minerals could inevitably coprecipitate and interact with jarosite structure), may play a role in the releasing behavior [89]. But further investigations are required to reveal the exact retention mechanism.

With regard to the sulfate release, both experimental observations and simulation exhibit its virtual pH-independent leaching behavior within the acidic and neutral pH range (Fig.4d, from 1 to 6), with the concentrations remaining relatively constant at 10^4 μmol/L. The geochemical modeling reveals that in this pH range, gypsum, jarosite, and anglesite are the potential solubility-controlling minerals for SO_4^{2-} leaching. In contrast, an increased release of SO_4^{2-} was observed under alkaline conditions (Fig.4d, pH from 6 to 13), as the pH values are not suitable for the stability of gypsum, jarosite, and anglesite. Furthermore, although simulations with the jarosite dissolution limit (MO.2) reflect this upward trend successfully, deviations in SO_4^{2-} concentration can still be observed (Fig.4d). It is speculated that, in addition to overestimating the solubility of gypsum, SO_4^{2-} anions are absorbed or co-existed with newly formed ferrihydrite (Fig.S4) at neutral and alkaline conditions, as electrostatic forces at the surface-water interface play a vital role on sulfate adsorption mechanism [52]. Further research is needed to fully understand the complex interactions between the different factors affecting sulfate release.

4.3. Environmental risk

As demonstrated in previous sections, the concentrations and leachabilities of PTEs are strongly influenced by the pH values due to the different geochemical stabilities of the PTEs-containing species. Numerous studies have indicated that the high solubility of PTEs represents a greater potential risk of contamination to plants and humans, especially during the rainy period when the washout of soluble phases may occur [28,52]. Significantly, the complexity of the studied area (Fig.7c, coastline city, stockpiled near the surface, and sparse vegetation cover) and the subsequent exposure of the contaminants to various environmental conditions (e.g., wind, erosion, acid rain, proximity to groundwater/surface water), makes it crucial to monitor the site and carefully take appropriate measures to minimize the risks [30].

From the pH-dependent leaching tests (Fig.4a and b), it can be concluded that the optimum pH for the lowest solubility of Pb and Zn is near the pH range of 8–10. This is due to the synergistic effects deriving from the remained jarosite, the formation of Pb/Zn-bearing carbonates, and the assumed ferrihydrite precipitation contributing to significantly lower concentrations of Pb and Zn in the leachates (pH 9.04, Fig.5d). If the contaminated soil is kept at this pH range, a lower release of hazardous would be expected. Nonetheless, the concentrations of the released contaminants are still higher than the threshold limits (0.50×10^{-1} μmol/L for both Pb and Zn, from Decreto legislativo 3 aprile 2006, n. 152). In addition, field works in Italy revealed that the water from the rainfall and aquifers has a pH ranging from nearly neutral to slightly acidic [90,91], suggesting that the sorption/desorption of contaminants on ferrihydrite and carbonates may not govern the Pb and Zn retention in its natural stockpile state. Severe acid rain circumstances can also expose the risk of higher release of contaminants.

Hence, the outdated and improper stock is insufficient for the long-term disposal of contaminated soil, and efficient treatment is urgently needed for its management. Some works focused on the ex-situ immobilization technologies of these materials, for instance, ex-situ soil washing and filling [92], electrokinetic remediation [93], and chemical extraction [94]. For ex-situ treatment, it is fundamental to evaluate the advantages and disadvantages of the intervention and compare them with the scenario of leaving the contaminated soil in the current state. It has to be evaluated whether the environmental and human health risks outweigh the risks of re-opening the site, especially the potential secondary pollution caused by the excavation and transportation processes during the large-scale reprocessing plan. Alternative approaches encompass in-situ remediation strategies, such as high-performance solidification/stabilization procedures [10] and cemented paste backfill [95], that could be envisaged for this contaminated soil. However, based on the amphoteric leaching behavior revealed by the pH-dependent leaching test, the traditional binders (ordinary Portland cement or lime) might not be suitable for the management scenarios. It is because the high alkalinity provided by traditional binders might increase the mobility of Pb and Zn under alkaline conditions (pH>10). Therefore, additional studies need to be conducted on the mix design, the buffering capacity, and the leaching potential of metals.

5. Conclusion

This study focused on assessing the leaching behavior and potential environmental risks of soil contaminated by Pb, Zn, and sulfates, mainly based on the geochemical mobility investigation and mineralogical assessments of the hazardous contaminants. The overall results demonstrated that Pb, Zn, and SO_4^{2-} are highly mobile in the studied pH range and that various mechanisms played a role in controlling the PTEs releasing behavior. With the aid of PHREEQC modeling, a more comprehensive mineralogical insight was provided into contaminated soil management-, which indicated that the forward model construction is feasible and capable of monitoring major and minor phases involved in PTEs retention. Overall, the combined use of geochemical modeling and experiments has prompted the possibility of an in-depth investigation for application to in-situ remediation in industrial sites. Moreover, this approach allows for the integration of experimental approaches to monitor the PTEs leaching behavior through a relatively uncomplicated pathway. The main findings are as follows:

(1) With the raw material characterization, anglesite and kintoreite are the main Pb-bearing crystalline phases detected in the XRD patterns, which may be generated from the oxidation of remaining pyrite particles. The sulfates (jarosite) were confirmed as the trace metal-bearing phases, as the Pb/Zn-Fe sulfates were characterized along the edge of the hematite particles. The SI estimation suggests that Pb and Zn preservation are associated with different phases and an adsorption mechanism is also active in the soil.

(2) The measured concentrations of PTEs in the leachates showed a strong dependence on the pH values of the contact solution. Both Pb and Zn releases exhibit an amphoteric behavior, with a downward trend at pH values of 8–10. The mineralogical information indicates that the solubility of trace metal compounds, especially in the form of oxides, hydroxides, and carbonates, significantly depends on the pH value. At acid conditions, the solubility of Pb is dominated by the dissolution of anglesite and the formation of Pb nitrate complexes, while Zn is controlled by Zn ions and Zn-sulfate complexes in the solution. The decrease of trace metal leaching in the neutral/alkaline region is related to the precipitation of carbonates and the potential adsorption onto jarosite and ferrihydrite. When the pH values move to strong alkaline conditions, the upward trend could be associated with the complexation of aqueous metal hydrates. Sulfate leaching is approximately constant in the pH range of 1–6, but increases at pH values above 7 due to the dissolution of gypsum, jarosite, and anglesite.

(3) The simulated and experimental results of leaching and

mineralogical composition of the residues are in good agreement. The conceptual model, which combined processes of precipitation/dissolution and formation of solid solutions, gave a great reproduction of the amphoteric Pb and Zn leaching. The jarosite was preserved in the residues, which could be related to the formation of nanoparticles of secondary iron oxide phases. Limited by the lack of appropriate thermodynamic data for highly-soluble gypsum, its dissolution at alkaline conditions is over-estimated, which should be considered for further optimization. But the general estimation has progressed in the ability to predict the environmental fates of associated PTEs.

(4) The concern over PTEs' pH-dependent mobility highlights the severe risk to both the environment and human health posed by contaminated soil, even in its natural state. This risk only becomes more pronounced under acidic or alkaline conditions. Geochemical modeling provides in-depth information about the contribution of specific PTEs' solubility-controlling phases to the risk, thus offering new perspectives for improved predictions and constraints on PTE release.

CRediT authorship contribution statement

Yikai Liu: Conceptualization, Writing – original draft preparation, Investigation, Formal analysis. **Simone Molinari:** Conceptualization, Validation, Writing – review & editing, Visualization. **Maria Chiara Dalconi:** Validation, Investigation, Visualization, Writing – review & editing. **Luca Valentini:** Investigation, Validation, Visualization. **Giulia Ricci:** Investigation, Supervision. **Claudio Carrer:** Investigation, Validation. **Giorgio Ferrari:** Resources, Supervision. **Gilberto Artioli:** Conceptualization, Writing – review & editing, Project administration, Resources, Supervision, Validation.

Declaration of Competing Interest

The authors declare that they have no known competing financial interests or personal relationships that could have appeared to influence the work reported in this paper.

Data Availability

Data will be made available on request.

Acknowledgments

This study was conducted with financial support from the PRIN project "Mineral reactivity, a key to understand large-scale processes: from rock-forming environments to solid waste recovering/lithification" (No.2017L83S77) and a scholarship granted by the China Scholarship Council (No.CSC201906370062).

Appendix A. Supporting information

Supplementary data associated with this article can be found in the online version at doi:10.1016/j.jece.2023.109687.

References

[1] G.M. Filippelli, D. Morrison, D. Cicchella, Urban geochemistry and human health, Elements 8 (2012) 439–444, https://doi.org/10.2113/GSELEMENTS.8.6.439.
[2] O. Abollino, M. Aceto, M. Malandrino, E. Mentasti, C. Sarzanini, F. Petrella, Heavy metals in agricultural soils from Piedmont, Italy. Distribution, speciation and chemometric data treatment, Chemosphere 49 (2002) 545–557, https://doi.org/10.1016/S0045-6535(02)00352-1.
[3] D. Hou, D. O'Connor, A.D. Igalavithana, D.S. Alessi, J. Luo, D.C.W. Tsang, D.L. Sparks, Y. Yamauchi, J. Rinklebe, Y.S. Ok, Metal contamination and bioremediation of agricultural soils for food safety and sustainability, Nat. Rev. Earth Environ. 2020 17. 1 (2020) 366–381. https://doi.org/10.1038/s43017–020-0061-y.
[4] J.A. Torres-Martínez, A. Mora, P.S.K. Knappett, N. Ornelas-Soto, J. Mahlknecht, Tracking nitrate and sulfate sources in groundwater of an urbanized valley using a multi-tracer approach combined with a Bayesian isotope mixing model, Water Res. 182 (2020), 115962, https://doi.org/10.1016/J.WATRES.2020.115962.
[5] M.L.S. Oliveira, C.R. Ward, M. Izquierdo, C.H. Sampaio, I.A.S. de Brum, R. M. Kautzmann, S. Sabedot, X. Querol, L.F.O. Silva, Chemical composition and minerals in pyrite ash of an abandoned sulphuric acid production plant, Sci. Total Environ. 430 (2012) 34–47, https://doi.org/10.1016/J.SCITOTENV.2012.04.046.
[6] S. Bisone, M. Gautier, V. Chatain, D. Blanc, Spatial distribution and leaching behavior of pollutants from phosphogypsum stocked in a gypstack: geochemical characterization and modeling, J. Environ. Manag. (2017), https://doi.org/10.1016/j.jenvman.2017.02.055.
[7] H.P. Jambhulkar, S.M.S. Shaikh, M.S. Kumar, Fly ash toxicity, emerging issues and possible implications for its exploitation in agriculture; Indian scenario: a review, Chemosphere 213 (2018) 333–344, https://doi.org/10.1016/J.CHEMOSPHERE.2018.09.045.
[8] J. Kumpiene, J. Antelo, E. Brännvall, I. Carabante, K. Ek, M. Komárek, C. Söderberg, L. Wårell, In situ chemical stabilization of trace element-contaminated soil – Field demonstrations and barriers to transition from laboratory to the field – a review, Appl. Geochem. 100 (2019) 335–351, https://doi.org/10.1016/J.APGEOCHEM.2018.12.003.
[9] K.N. Palansooriya, S.M. Shaheen, S.S. Chen, D.C.W. Tsang, Y. Hashimoto, D. Hou, N.S. Bolan, J. Rinklebe, Y.S. Ok, Soil amendments for immobilization of potentially toxic elements in contaminated soils: a critical review, Environ. Int. 134 (2020), 105046, https://doi.org/10.1016/J.ENVINT.2019.105046.
[10] S. Contessi, L. Calgaro, M.C. Dalconi, A. Bonetto, M. Pietro Bellotto, G. Ferrari, A. Marcomini, G. Artioli, Stabilization of lead contaminated soil with traditional and alternative binders, J. Hazard. Mater. (2020), https://doi.org/10.1016/j.jhazmat.2019.120990.
[11] A. Ausili, L. Bergamin, E. Romano, Environmental status of Italian coastal marine areas affected by long history of contamination, Front. Environ. Sci. (2020), https://doi.org/10.3389/fenvs.2020.00034.
[12] A.C. Agnello, M. Bagard, E.D. van Hullebusch, G. Esposito, D. Huguenot, Comparative bioremediation of heavy metals and petroleum hydrocarbons co-contaminated soil by natural attenuation, phytoremediation, bioaugmentation and bioaugmentation-assisted phytoremediation, Sci. Total Environ. 563–564 (2016) 693–703, https://doi.org/10.1016/J.SCITOTENV.2015.10.061.
[13] E. Obeng-Gyasi, J. Roostaei, J.M. Gibson, Lead distribution in urban soil in a medium-sized city: household-scale analysis, Environ. Sci. Technol. 55 (2021) 3696–3705, https://doi.org/10.1021/ACS.EST.0C07317/SUPPL_FILE/ES0C07317_SI_001.PDF.
[14] M.J. Kang, S. Yu, S.W. Jeon, M.C. Jung, Y.K. Kwon, P.K. Lee, G. Chae, Mobility of metal(loid)s in roof dusts and agricultural soils surrounding a Zn smelter: focused on the impacts of smelter-derived fugitive dusts, Sci. Total Environ. 757 (2021), 143884, https://doi.org/10.1016/J.SCITOTENV.2020.143884.
[15] M. Tuhý, T. Hrstka, V. Ettler, Automated mineralogy for quantification and partitioning of metal(loid)s in particulates from mining/smelting-polluted soils, Environ. Pollut. 266 (2020), 115118, https://doi.org/10.1016/J.ENVPOL.2020.115118.
[16] G. Izydorczyk, K. Mikula, D. Skrzypczak, K. Moustakas, A. Witek-Krowiak, K. Chojnacka, Potential environmental pollution from copper metallurgy and methods of management, Environ. Res. 197 (2021), 111050, https://doi.org/10.1016/J.ENVRES.2021.111050.
[17] A.S.M. Fazle Bari, D. Lamb, G. Choppala, B. Seshadri, M.R. Islam, P. Sanderson, M. M. Rahman, Arsenic bioaccessibility and fractionation in abandoned mine soils from selected sites in New South Wales, Australia and human health risk assessment, Ecotoxicol. Environ. Saf. 223 (2021), 112611, https://doi.org/10.1016/J.ECOENV.2021.112611.
[18] D.M. Xu, R.B. Fu, J.X. Wang, B.H. An, The geochemical behaviors of potentially toxic elements in a typical lead/zinc (Pb/Zn) smelter contaminated soil with quantitative mineralogical assessments, J. Hazard. Mater. (2022), https://doi.org/10.1016/j.jhazmat.2021.127127.
[19] L. Poggio, B. Vrščaj, R. Schulin, E. Hepperle, F. Ajmone Marsan, Metals pollution and human bioaccessibility of topsoils in Grugliasco (Italy), Environ. Pollut. 157 (2009) 680–689, https://doi.org/10.1016/J.ENVPOL.2008.08.009.
[20] F. Jiao, L. Zhang, Z. Dong, T. Namioka, N. Yamada, Y. Ninomiya, Study on the species of heavy metals in MSW incineration fly ash and their leaching behavior, Fuel Process. Technol. 152 (2016) 108–115, https://doi.org/10.1016/J.FUPROC.2016.06.013.
[21] T.V. Rakotonimaro, M. Guittony, C.M. Neculita, Compaction of peat cover over desulfurized gold mine tailings changes: arsenic speciation and mobility, Appl. Geochem. 128 (2021), 104923, https://doi.org/10.1016/J.APGEOCHEM.2021.104923.
[22] M. Gabarrón, O. Babur, J.M. Soriano-Disla, A. Faz, J.A. Acosta, Composition and risk assessment of roasted pyrite ash from fertiliser production, Chemosphere 209 (2018) 277–285, https://doi.org/10.1016/J.CHEMOSPHERE.2018.06.109.
[23] J. Deng, K. Zhang, D. He, H. Zhao, R. Hakkou, M. Benzaazoua, Occurrence of sesquioxide in a mid-low grade collophane-sedimentary apatite ore from guizhou, china, Minerals (2020), https://doi.org/10.3390/min10111038.
[24] S. Contessi, M.C. Dalconi, S. Pollastri, L. Calgaro, C. Meneghini, G. Ferrari, A. Marcomini, G. Artioli, Cement-stabilized contaminated soil: Understanding Pb retention with XANES and Raman spectroscopy, Sci. Total Environ. 752 (2021), 141826, https://doi.org/10.1016/J.SCITOTENV.2020.141826.
[25] S. Zhou, X. Li, Y. Zhou, C. Min, Y. Shi, Effect of phosphorus on the properties of phosphogypsum-based cemented backfill, J. Hazard. Mater. (2020), https://doi.org/10.1016/j.jhazmat.2020.122993.
[26] C.B. Tabelin, R.D. Corpuz, T. Igarashi, M. Villacorte-Tabelin, R.D. Alorro, K. Yoo, S. Raval, M. Ito, N. Hiroyoshi, Acid mine drainage formation and arsenic mobility

under strongly acidic conditions: importance of soluble phases, iron oxyhydroxides/oxides and nature of oxidation layer on pyrite, J. Hazard. Mater. 399 (2020), 122844, https://doi.org/10.1016/J.JHAZMAT.2020.122844.
[27] H. Khan, A.S. Yerramilli, A. D'Oliveira, T.L. Alford, D.C. Boffito, G.S. Patience, Experimental methods in chemical engineering: X-ray diffraction spectroscopy—XRD, Can. J. Chem. Eng. 98 (2020) 1255–1266, https://doi.org/10.1002/CJCE.23747.
[28] A. Pękala, M. Musiał, Modelling the leachability of strontium and barium from stone building materials, Materials 14 (2021), https://doi.org/10.3390/MA14123403.
[29] B. Guo, Y. Xiong, W. Chen, S.A. Saslow, N. Kozai, T. Ohnuki, I. Dabo, K. Sasaki, Spectroscopic and first-principles investigations of iodine species incorporation into ettringite: implications for iodine migration in cement waste forms, J. Hazard. Mater. 389 (2020), 121880, https://doi.org/10.1016/J.JHAZMAT.2019.121880.
[30] J. Helser, E. Vassilieva, V. Cappuyns, Environmental and human health risk assessment of sulfidic mine waste: bioaccessibility, leaching and mineralogy, J. Hazard. Mater. 424 (2022), 127313, https://doi.org/10.1016/J.JHAZMAT.2021.127313.
[31] V. Cappuyns, V. Alian, E. Vassilieva, R. Swennen, PH dependent leaching behavior of Zn, Cd, Pb, Cu and As from mining wastes and slags: Kinetics and mineralogical control, Waste Biomass Valoriz. 5 (2014) 355–368, https://doi.org/10.1007/S12649-013-9274-3/FIGURES/5.
[32] H. Wei, Y. Liu, J. Zhang, S. Li, X. Zhong, H. Xiang, Leaching of simulated acid rain deteriorates soil physiochemical and mechanical properties in three agricultural soils, Catena 206 (2021), 105485, https://doi.org/10.1016/J.CATENA.2021.105485.
[33] J.J. Dijkstra, R.N.J. Comans, J. Schokker, M.J. van der Meulen, The geological significance of novel anthropogenic materials: Deposits of industrial waste and by-products, Anthropocene 28 (2019), 100229, https://doi.org/10.1016/J.ANCENE.2019.100229.
[34] British Standards Institution, Characterisation of Waste - Leaching - Compliance Test for Leaching of Granular Waste Materials and Sludges - Part 4: One Stage Batch Test at a Liquid to Solid Ratio of 10 l/kg for Materials With Particle Size Below 10 Mm (without or With Size Reduction), (2004).
[35] C. Bettiol, L. Stievano, M. Bertelle, F. Delfino, E. Argese, Evaluation of microwave-assisted acid extraction procedures for the determination of metal content and potential bioavailability in sediments, Appl. Geochem. 23 (2008) 1140–1151, https://doi.org/10.1016/J.APGEOCHEM.2007.11.008.
[36] E. Gliozzo, M.C. Dalconi, G. Cruciani, I.T. Memmi, Application of the Rietveld method for the investigation of mortars: a case study on the archaeological site of Thamusida (Morocco), Eur. J. Miner. 21 (2009) 457–465, https://doi.org/10.1127/0935-1221/2009/0021-1905.
[37] H.M. Rietveld, A profile refinement method for nuclear and magnetic structures, J. Appl. Crystallogr. 2 (1969) 65–71, https://doi.org/10.1107/S0021889869006558.
[38] N. Doebelin, R. Kleeberg, Profex: a graphical user interface for the Rietveld refinement program BGMN, Urn:Issn:1600–5767. 48 (2015) 1573–1580. https://doi.org/10.1107/S1600576715014685.
[39] D.L. Parkhurst, C.A.J. Appelo, Description of Input and Examples for PHREEQC Version 3 — A Computer Program for Speciation, Batch-Reaction, One-Dimensional Transport, and Inverse Geochemical Calculations., U.S. Geol. Surv. Tech. Methods, B. 6, Chapter A43. (2013).
[40] J.P. Gustafsson, Vis. MINTEQ 3. 1 Use Guide, Dep. L. Water Recources, Stock. Swed. 2011 1 73.
[41] D. Bernasconi, C. Caviglia, E. Destefanis, A. Agostino, R. Boero, N. Marinoni, C. Bonadiman, A. Pavese, Influence of speciation distribution and particle size on heavy metal leaching from MSWI fly ash, Waste Manag 138 (2022) 318–327, https://doi.org/10.1016/J.WASMAN.2021.12.008.
[42] J.J. Dijkstra, H.A. Van Der Sloot, R.N.J. Comans, The leaching of major and trace elements from MSWI bottom ash as a function of pH and time, Appl. Geochem. 21 (2006) 335–351, https://doi.org/10.1016/J.APGEOCHEM.2005.11.003.
[43] M. Shi, X. Min, C. Tian, T. Hao, S. Zhu, Y. Ge, Q. Wang, X. Yan, Z. Lin, Mechanisms of Pb(II) coprecipitation with natrojarosite and its behavior during acid dissolution, J. Environ. Sci. 122 (2022) 128–137, https://doi.org/10.1016/J.JES.2021.10.006.
[44] J. Aguilar-Carrillo, L. Herrera, E.J. Gutiérrez, I.A. Reyes-Domínguez, Solid-phase distribution and mobility of thallium in mining-metallurgical residues: environmental hazard implications, Environ. Pollut. 243 (2018) 1833–1845, https://doi.org/10.1016/J.ENVPOL.2018.10.014.
[45] R.L. Frost, R.A. Wills, M.L. Weier, W. Martens, S. Mills, A Raman spectroscopic study of selected natural jarosites, Spectrochim. Acta Part A Mol. Biomol. Spectrosc. 63 (2006) 1–8, https://doi.org/10.1016/J.SAA.2005.03.034.
[46] R.L. Frost, M.L. Weier, W. Martens, S. Mills, ThermoRaman spectroscopic study of kintoreite, Spectrochim. Acta Part A Mol. Biomol. Spectrosc. 63 (2006) 282–288, https://doi.org/10.1016/J.SAA.2005.05.011.
[47] R.L. Frost, R.A. Wills, M.L. Weier, W. Martens, Comparison of the Raman spectra of natural and synthetic K- and Na-jarosites at 298 and 77 K, J. Raman Spectrosc. 36 (2005) 435–444, https://doi.org/10.1002/JRS.1317.
[48] K. Chen, X. Jin, C. Guo, C. He, Y. Zhang, K. Gao, G. Lu, Z. Dang, Reductive dissolution of Pb-Zn jarosite under near-neutral conditions, Chem. Geol. 579 (2021), 120338, https://doi.org/10.1016/J.CHEMGEO.2021.120338.
[49] K. Sasaki1, O. Tanaike, H. Konno, Distinction of jarosite-group compounds by Raman spectroscopy, Can. Mineral. 36 (1998) 1225–1235.
[50] F.L. Forray, A.M.L. Smith, A. Navrotsky, K. Wright, K.A. Hudson-Edwards, W. E. Dubbin, Synthesis, characterization and thermochemistry of synthetic Pb–As, Pb–Cu and Pb–Zn jarosites, Geochim. Cosmochim. Acta 127 (2014) 107–119, https://doi.org/10.1016/J.GCA.2013.10.043.
[51] A. Jarošíková, V. Ettler, M. Mihaljevič, B. Kříbek, B. Mapani, The pH-dependent leaching behavior of slags from various stages of a copper smelting process: environmental implications, J. Environ. Manag. 187 (2017) 178–186, https://doi.org/10.1016/J.JENVMAN.2016.11.037.
[52] J. Helser, V. Cappuyns, Trace elements leaching from PbZn mine waste (Plombières, Belgium) and environmental implications, J. Geochem. Explor. 220 (2021), 106659, https://doi.org/10.1016/J.GEXPLO.2020.106659.
[53] F. Nikkhou, F. Xia, M. Knorsch, A.P. Deditius, Mechanisms of surface passivation during galena leaching by hydrogen peroxide in acetate and citrate solutions at 25-50 °c, ACS Sustain. Chem. Eng. 8 (2020) 14407–14416, https://doi.org/10.1021/ACSSUSCHEMENG.0C04272/SUPPL_FILE/SC0C04272_SI_001.PDF.
[54] A. Kölbl, K. Kaiser, P. Winkler, L. Mosley, R. Fitzpatrick, P. Marschner, F. E. Wagner, W. Häusler, R. Mikutta, Transformation of jarosite during simulated remediation of a sandy sulfuric soil, Sci. Total Environ. 773 (2021), 145546, https://doi.org/10.1016/J.SCITOTENV.2021.145546.
[55] A.M.L. Smith, K.A. Hudson-Edwards, W.E. Dubbin, K. Wright, Dissolution of jarosite [KFe3(SO4)2(OH)6] at pH 2 and 8: insights from batch experiments and computational modelling, Geochim. Cosmochim. Acta 70 (2006) 608–621, https://doi.org/10.1016/J.GCA.2005.09.024.
[56] B. Han, B. Altansukh, K. Haga, Z. Stevanović, R. Jonović, L. Avramović, D. Urosević, Y. Takasaki, N. Masuda, D. Ishiyama, A. Shibayama, Development of copper recovery process from flotation tailings by a combined method of high—pressure leaching—solvent extraction, J. Hazard. Mater. 352 (2018) 192–203. https://doi.org/10.1016/J.JHAZMAT.2018.03.014.
[57] A. Navarro, E. Cardellach, M. Corbella, Immobilization of Cu, Pb and Zn in mine-contaminated soils using reactive materials, J. Hazard. Mater. 186 (2011) 1576–1585, https://doi.org/10.1016/J.JHAZMAT.2010.12.039.
[58] M. Vítková, V. Ettler, O. Šebek, M. Mihaljevič, T. Grygar, J. Rohovec, The pH-dependent leaching of inorganic contaminants from secondary lead smelter fly ash, J. Hazard. Mater. 167 (2009) 427–433, https://doi.org/10.1016/J.JHAZMAT.2008.12.136.
[59] P. Tangviroon, K. Noto, T. Igarashi, T. Kawashima, M. Ito, T. Sato, W. Mufalo, M. Chirwa, I. Nyambe, H. Nakata, S. Nakayama, M. Ishizuka, Immobilization of Lead and Zinc Leached from Mining Residual Materials in Kabwe, Zambia: Possibility of Chemical Immobilization by Dolomite, Calcined Dolomite, and Magnesium Oxide, Miner. 2020, Vol. 10, Page 763. 10 (2020) 763. https://doi.org/10.3390/MIN10090763.
[60] M. Redwan, D. Rammlmair, K. Berkh, Secondary minerals in a calcareous environment: an example from Um Gheig Pb/Zn mine site, Eastern Desert, Egypt, Environ. Earth Sci. 80 (2021) 1–19, https://doi.org/10.1007/S12665-021-09590-X/FIGURES/10.
[61] H. Garbaya, A. Jraba, M.A. Khadimallah, E. Elaloui, The development of a new phosphogypsum-based construction material: A study of the physicochemical, mechanical and thermal characteristics, Materials 14 (2021), https://doi.org/10.3390/MA14237369.
[62] R. El Zrelli, L. Rabaoui, N. Daghbouj, H. Abda, S. Castet, C. Josse, P. van Beek, M. Souhaut, S. Michel, N. Bejaoui, P. Courjault-Radé, Characterization of phosphate rock and phosphogypsum from Gabes phosphate fertilizer factories (SE Tunisia): high mining potential and implications for environmental protection, Environ. Sci. Pollut. Res. 25 (2018) 14690–14702, https://doi.org/10.1007/s11356-018-1648-4.
[63] R. Pérez-López, R. Sáez, A.M. Álvarez-Valero, J.M. Nieto, G. Pace, Combination of sequential chemical extraction and modelling of dam-break wave propagation to aid assessment of risk related to the possible collapse of a roasted sulphide tailings dam, Sci. Total Environ. 407 (2009) 5761–5771, https://doi.org/10.1016/J.SCITOTENV.2009.07.031.
[64] Y. Liu, D. Guo, L. Dong, Y. Xu, J. Liu, Pollution status and environmental sound management (ESM) trends on typical general industrial solid waste, Procedia Environ. Sci. 31 (2016) 615–620, https://doi.org/10.1016/J.PROENV.2016.02.111.
[65] D. Bendz, C. Tiberg, D.B. Kleja, Mineralogical characterization and speciation of sulfur, zinc and lead in pyrite cinder from Bergvik, Sweden, Appl. Geochem. 131 (2021), 105010, https://doi.org/10.1016/J.APGEOCHEM.2021.105010.
[66] C. Yang, Y. Chen, P. Peng, C. Li, X. Chang, Y. Wu, Trace element transformations and partitioning during the roasting of pyrite ores in the sulfuric acid industry, J. Hazard. Mater. 167 (2009) 835–845, https://doi.org/10.1016/J.JHAZMAT.2009.01.067.
[67] S.C. Qin, K.X. Jiang, H.B. Wang, B.S. Zhang, Y.F. Wang, X.D. Zhang, Research on Behavior of Iron in the Zinc Sulfide Pressure Leaching Process, Miner. 2020, Vol. 10, Page 224. 10 (2020) 224. https://doi.org/10.3390/MIN10030224.
[68] F.L. Forray, A.M.L. Smith, C. Drouet, A. Navrotsky, K. Wright, K.A. Hudson-Edwards, W.E. Dubbin, Synthesis, characterization and thermochemistry of a Pb-jarosite, Geochim. Cosmochim. Acta 74 (2010) 215–224, https://doi.org/10.1016/J.GCA.2009.09.033.
[69] J. Aguilar-Carrillo, M. Villalobos, T. Pi-Puig, I.N. Escobar-Quiroz, F.M. Romero, Synergistic arsenic(v) and lead(ii) retention on synthetic jarosite. I. Simultaneous structural incorporation behaviour and mechanism, Environ. Sci. Process. Impacts 20 (2018) 354–369, https://doi.org/10.1039/C7EM00426E.
[70] R. Li, Q. Li, X. Sun, J. Li, J. Shen, W. Han, L. Wang, Removal of lead complexes by ferrous phosphate and iron phosphate: Unexpected favorable role of ferrous ions, J. Hazard. Mater. 392 (2020), 122509, https://doi.org/10.1016/J.JHAZMAT.2020.122509.

[71] N.C. Munksgaard, B.G. Lottermoser, Fertilizer amendment of mining-impacted soils from broken hill, Water Air Soil Pollut (2011) 373–397, https://doi.org/10.1007/S11270-010-0485-Y/FIGURES/11.
[72] M. Schindler, M.F. Hochella, Sequestration of Pb–Zn–Sb- and As-bearing incidental nanoparticles by mineral surface coatings and mineralized organic matter in soils, Environ. Sci. Process. Impacts 19 (2017) 1016–1027, https://doi.org/10.1039/C7EM00202E.
[73] Radana Malíková Vrtiška Luboš, Zajímavý Jiří Sejkora, výskyt fosfátů v okolí Líštěnce u Votic (Česká republika), Bull. Miner. Odd. Nár. Muz. 24 (2016) 114–131.
[74] D. Mauro, C. Biagioni, F. Zaccarini, A contribution to the mineralogy of Sicily, Italy – Kintoreite from the Tripi mine, Peloritani Mountains: occurrence and crystal structure, Mineral. Mag. 55 (2021) 1–9, https://doi.org/10.1180/MGM.2021.85.
[75] S. Xuexin, Minor elements and ore genesis of the Fankou lead-zinc deposit, China, Miner. Depos. 1984 192. 19 (1984) 95–104. https://doi.org/10.1007/BF00204667.
[76] J.A. Carrero, N. Goienaga, M. Olivares, I. Martinez-Arkarazo, G. Arana, J. M. Madariaga, Raman spectroscopy assisted with XRF and chemical simulation to assess the synergic impacts of guardrails and traffic pollutants on urban soils, J. Raman Spectrosc. 43 (2012) 1498–1503, https://doi.org/10.1002/JRS.4089.
[77] C. Yang, G. Lu, Y. Xie, L. Guo, M. Chen, L. Ge, Z. Dang, Sulfate migration and transformation characteristics in paddy soil profile affected by acid mine drainage, Environ. Res. 200 (2021), 111732, https://doi.org/10.1016/J.ENVRES.2021.111732.
[78] A. Król, K. Mizerna, M. Bożym, An assessment of pH-dependent release and mobility of heavy metals from metallurgical slag, J. Hazard. Mater. 384 (2020), 121502, https://doi.org/10.1016/J.JHAZMAT.2019.121502.
[79] C.J. Engelsen, H.A. Van Der Sloot, G. Wibetoe, H. Justnes, W. Lund, E. Stoltenberg-Hansson, Leaching characterisation and geochemical modelling of minor and trace elements released from recycled concrete aggregates, Cem. Concr. Res. 40 (2010) 1639–1649, https://doi.org/10.1016/J.CEMCONRES.2010.08.001.
[80] Q. Tian, B. Guo, S. Nakama, K. Sasaki, Distributions and leaching behaviors of toxic elements in fly ash, ACS Omega 3 (2018) 13055–13064, https://doi.org/10.1021/ACSOMEGA.8B02096/ASSET/IMAGES/ACSOMEGA.8B02096.SOCIAL.JPEG_V03.
[81] A.A. Rouff, R.J. Reeder, N.S. Fisher, Electrolyte and pH effects on Pb(II)–calcite sorption processes: the role of the PbCO03(aq) complex, J. Colloid Interface Sci. 286 (2005) 61–67, https://doi.org/10.1016/J.JCIS.2005.01.053.
[82] V. Ettler, M. Mihaljevič, O. Šebek, T. Grygar, Assessment of single extractions for the determination of mobile forms of metals in highly polluted soils and sediments—analytical and thermodynamic approaches, Anal. Chim. Acta 602 (2007) 131–140, https://doi.org/10.1016/J.ACA.2007.09.017.
[83] V. Ettler, D. Štěpánek, M. Mihaljevič, P. Drahota, R. Jedlicka, B. Kříbek, A. Vaněk, V. Penížek, O. Sracek, I. Nyambe, Slag dusts from Kabwe (Zambia): contaminant mineralogy and oral bioaccessibility, Chemosphere 260 (2020), 127642, https://doi.org/10.1016/J.CHEMOSPHERE.2020.127642.
[84] J. Reichert, G. Borg, Numerical simulation and a geochemical model of supergene carbonate-hosted non-sulphide zinc deposits, Ore Geol. Rev. 33 (2008) 134–151, https://doi.org/10.1016/J.OREGEOREV.2007.02.006.
[85] J.J. Dijkstra, J.C.L. Meeussen, R.N.J. Comans, Evaluation of a generic multisurface sorption model for inorganic soil contaminants, Environ. Sci. Technol. 43 (2009) 6196–6201, https://doi.org/10.1021/ES900555G/SUPPL_FILE/ES900555G_SI_001.PDF.
[86] C. Ye, P.A. Ariya, F. Fu, G. Yu, B. Tang, Influence of Al(III) and Sb(V) on the transformation of ferrihydrite nanoparticles: interaction among ferrihydrite, coprecipitated Al(III) and Sb(V), J. Hazard. Mater. 408 (2021), 124423, https://doi.org/10.1016/J.JHAZMAT.2020.124423.
[87] E.J. Bylaska, J.G. Catalano, S.T. Mergelsberg, S.A. Saslow, O. Qafoku, M.P. Prange, E.S. Ilton, Association of Defects and Zinc in Hematite, Environ. Sci. Technol. 53 (2019) 13687–13694, https://doi.org/10.1021/ACS.EST.9B04323/ASSET/IMAGES/LARGE/ES9B04323_0004.JPEG.
[88] J. Liu, R. Zhu, T. Xu, Y. Xu, F. Ge, Y. Xi, J. Zhu, H. He, Co-adsorption of phosphate and zinc(II) on the surface of ferrihydrite, Chemosphere 144 (2016) 1148–1155, https://doi.org/10.1016/J.CHEMOSPHERE.2015.09.083.
[89] M. Shi, X. Min, Y. Ke, Z. Lin, Z. Yang, S. Wang, N. Peng, X. Yan, S. Luo, J. Wu, Y. Wei, Recent progress in understanding the mechanism of heavy metals retention by iron (oxyhydr)oxides, Sci. Total Environ. 752 (2021), 141930, https://doi.org/10.1016/J.SCITOTENV.2020.141930.
[90] D. Di Curzio, S. Rusi, A. Di Giovanni, E. Ferretti, Evaluation of Groundwater Resources in Minor Plio-Pleistocene Arenaceous Aquifers in Central Italy, Hydrol. 2021, Vol. 8, Page 121. 8 (2021) 121. https://doi.org/10.3390/HYDROLOGY8030121.
[91] P. Madonia, G. Campilongo, M. Cangemi, M.L. Carapezza, S. Inguaggiato, M. Ranaldi, F. Vita, Hydrogeological and Geochemical Characteristics of the Coastal Aquifer of Stromboli Volcanic Island (Italy), Water 2021, Vol. 13, Page 417. 13 (2021) 417. https://doi.org/10.3390/W13040417.
[92] L. Liu, W. Li, W. Song, M. Guo, Remediation techniques for heavy metal-contaminated soils: Principles and applicability, Sci. Total Environ. (2018), https://doi.org/10.1016/j.scitotenv.2018.03.161.
[93] K.B. Pedersen, P.E. Jensen, L.M. Ottosen, J. Barlindhaug, Influence of electrode placement for mobilising and removing metals during electrodialytic remediation of metals from shooting range soil, Chemosphere 210 (2018) 683–691, https://doi.org/10.1016/J.CHEMOSPHERE.2018.07.063.
[94] Y. Zhang, C. Labianca, L. Chen, S. De Gisi, M. Notarnicola, B. Guo, J. Sun, S. Ding, L. Wang, Sustainable ex-situ remediation of contaminated sediment: a review, Environ. Pollut. 287 (2021), 117333, https://doi.org/10.1016/J.ENVPOL.2021.117333.
[95] Z. Guo, J. Qiu, H. Jiang, S. Zhang, H. Ding, Improving the performance of superfine-tailings cemented paste backfill with a new blended binder, Powder Technol. 394 (2021) 149–160, https://doi.org/10.1016/J.POWTEC.2021.08.029.